

On the Clustering of Lyman Alpha Clouds

Renyue Cen¹, Steven Phelps², Jordi Miralda-Escudé³ and Jeremiah P. Ostriker⁴

Received _____; accepted _____

arXiv:astro-ph/9709108v1 11 Sep 1997

¹Princeton University Observatory, Princeton University, Princeton, NJ 08544;
cen@astro.princeton.edu

²Department of Physics, Princeton University, Princeton, NJ 08544;
phelps@astro.princeton.edu

³Department of Physics and Astronomy, University of Pennsylvania;
jordi@llull.physics.upenn.edu

⁴Princeton University Observatory, Princeton University, Princeton, NJ 08544;
jpo@astro.princeton.edu

ABSTRACT

We examine the correlational property of Ly α clouds (along the line of sight) in detail utilizing a hydrodynamic simulation of Ly α clouds in a cold dark matter universe with a cosmological constant, and compare it to that of mass and galaxies. We show that the correlation strength of Ly α clouds is somewhat weaker than that of the underlying matter, which in turn should be weaker than that of galaxies (biased galaxy formation). On the scales probed, 10 – 300km/s, for Ly α clouds we find that higher density, higher optical depth, higher column density regions are more strongly clustered than lower density, lower optical depth, lower column density regions, with the difference being larger at small separations and smaller at large separations. Thus, a consistent picture seems to emerge: the correlation strength for a given set of objects is positively correlated with their characteristic global density and the differences among the correlations of galaxies, Ly α clouds and mass reflect the differences in density that each trace. Significant positive correlations with a strength of 0.1 – 1.0 are found for Ly α clouds in the velocity range 50 – 300km/s. This effect should be observable. The correlation function of Ly α clouds seems to be a monotonically decreasing function of separation, indicating that correlation strength should be less than 0.1 at $\Delta v > 300$ km/s, where our current simulation box is too small to give a reliable measure.

Among the correlational measures examined, an optical depth correlation function (Equation 5) proposed here may serve as the best correlational measure. It reasonably faithfully represents the true correlation of the underlying matter, enabling a better indication of both matter correlation and the relationship between galaxies and Ly α clouds. Furthermore, it appears to be an alternative to the conventional line-line correlation function with the virtue that it does not

require ambiguous post-observation fitting procedures such as those commonly employed in the conventional line-finding methods. Neither does it depend sensitively on the observational resolution (e.g., FWHM), insofar as the clouds are resolved (i.e., the FWHM is smaller than the line width). Conveniently, it can be easily measured with the current observational sensitivity without being contaminated significantly by the presence of noise, if one chooses an appropriate optical depth floor value τ_{min} (an adjustable parameter) say, ≤ 2.0 .

Subject headings: Cosmology: large-scale structure of Universe – cosmology: theory – intergalactic medium – quasars: absorption lines – hydrodynamics

1. Introduction

With rapid advances in observational capabilities in recent years, thanks to the advent of the ground-based 10m Keck telescopes as well as the Hubble Space Telescope, observation of the Ly α forest has become a highly useful tool for probing the universe at low-to-moderate redshift (e.g., Carswell et al. 1991; Rauch et al. 1992; Petitjean et al. 1993; Schneider et al. 1993; Cristiani et al. 1995; Hu et al. 1995; Tytler et al. 1995; Lanzetta et al. 1995; Bahcall et al. 1996). When analyzed in conjunction with progressively more sophisticated and accurate theoretical modelling (Cen et al. 1994, CMOR hereafter; Zhang et al. 1995; Hernquist et al. 1996; Miralda-Escudé et al. 1996, MCOR hereafter), made possible by the availability of powerful computers and accurate cosmological hydrodynamic codes, observations of Ly α clouds should greatly enhance our ability to test cosmological models. The above quoted papers show such a good agreement between theory and observation with regard to physical properties which have already been documented, that we are led to use the theory now to predict properties, such as spatial correlations among Ly α clouds, that have not yet been reliably measured.

Early observations that Ly α clouds are very weakly clustered in velocity space on scales $\geq 300\text{km/s}$ along the line of sight to distant quasars at high redshift (Sargent et al. 1980), compared to the expected correlations among galaxies at the same redshift, provided the first compelling evidence that Ly α clouds at high redshift are perhaps not associated with galaxies. This single piece of evidence, combined with the inferred temperature of the clouds, has spawned most subsequent discussions about their origin and nature (Ostriker & Ikeuchi 1983; Ikeuchi & Ostriker 1986; Rees 1986; Ikeuchi 1986; Bond, Szalay, & Silk 1988). On the other hand, the recent observations by HST seem to indicate that Ly α clouds at low redshift ($z \leq 1.0$) may have their origin directly inside or in very close proximity to galaxies (Lanzetta et al. 1995; Bahcall et al. 1996). Of course, ground based moderate redshift

observations and space based low redshift observations may sample essentially different populations, since the high redshift population is declining with decreasing redshift at such a large rate as to make a negligible contribution to the HST observed lines. Moreover, various studies of the clustering of Ly α clouds at high redshift, which primarily measure line correlations along the line of sight, have arrived at different results. For example, Webb (1986) suggests that Ly α clouds are weakly clustered with $\langle \xi \rangle = 0.32 \pm 0.08$ over the velocity range 50 – 290km/s, while Rauch et al. (1992) find no clustering at any scale for the clouds as a whole. Such seemingly conflicting observational evidence at high redshift and between high and low redshifts indicate that our current understanding of the clustering properties of Ly α clouds may be quite incomplete.

In this paper we attempt to understand better the spatial clustering properties of Ly α clouds by analyzing the simulated Ly α clouds in the cold dark matter model with a cosmological constant (Λ CDM). This model, according to the MCOR analysis, provides a good fit to the observed distributions of absorption in the Ly α forest as measured by the one-point distribution function of transmitted flux, namely the flux distribution and the derived column density distribution, but that work did not examine the two-point correlation of the Ly α clouds in much detail. In the present work several clustering measures are used, including a line-line two-point correlation function and measures (some newly proposed) directly using flux and optical depth distributions as well as more fundamental matter correlations, directly computable in simulations. The paper is organized as follows: A brief description of the simulation is given in §2. The correlational measures used to analyze the simulation are defined in §3. Results and conclusions are given in §4 and §5.

2. Simulation

We simulate the formation of Ly α clouds in a spatially flat cold dark matter universe with a cosmological constant (Λ CDM), with the following cosmological parameters: Hubble constant $H_o = 65\text{km/s/Mpc}$, $\Omega_{0,CDM} = 0.3645$, $\Lambda_0 = 0.6$, $\Omega_{0,b} = 0.0355$ (cf. Walker et al. 1991), $\sigma_8 = 0.79$ (the simulations we use in this paper are the same as those used in CMOR and MCOR). The primary motivation for choosing this model is simple: overall it provides an excellent fit to available observations (Ostriker & Steinhardt 1995, "Concordance model"). The simulation box size is $10h^{-1}\text{Mpc}$ comoving with $N = 288^3$ cells and 144^3 dark matter particles. The cell size is $35 h^{-1}\text{kpc}$ (comoving) corresponding to an average baryonic cell mass of $6.3 \times 10^5 M_\odot$, with the true spatial and mass resolutions being about 2 and 8 times worse than those values, respectively. At $z = 3$, the Jeans length, $\lambda_J \equiv (\pi c_s^2 / G \bar{\rho}_{tot})^{1/2}$ for $c_s = v_{rms} = 10 \text{ km/s}$, is equal to $400h^{-1} \text{ kpc}$ in comoving units, or 11 cells. The power spectrum transfer function is computed using the method described in Cen, Gnedin, & Ostriker (1993). We use a new shock-capturing Total Variation Diminishing (TVD) cosmological hydrodynamic code described in Ryu et al. (1993).

All the atomic processes for a plasma of (H, He) of primeval composition (76%,24%) in mass are included, using the heating, cooling, and ionization terms described in Cen (1992). We calculate self-consistently the average background photoionizing radiation field as a function of frequency, assuming the radiation field is spatially uniform (i.e., optically thin). The evolution of the radiation field is calculated given the average attenuation in the simulated box and the emission (both from the gas itself and from the assumed sources of ionizing photons). The time-dependent equations for the ionization structure of the gas are solved by iteration using an implicit method, to avoid the instabilities that arise in solving stiff equations. In general, the abundances of different species are close to ionization equilibrium between recombination and photoionization after most of the gas has been

photoionized.

We model galaxy formation as in Cen & Ostriker (1992, 1993a,b). The material turning into collisionless particles as “galaxies” is assumed to emit ionizing radiation with two types of spectra: one characteristic of star formation regions and the other characteristic of quasars, with efficiencies (i.e., the fraction of rest-mass energy converted into radiation) of $e_{UV,*} = 5 \times 10^{-6}$, and $e_{UV,Q} = 6 \times 10^{-6}$, respectively. We adopt the emission spectrum of massive stars from Scalo (1986) and that of quasars from Edelson and Malkan (1986). These coefficients have been chosen to produce a computed radiation field consistent with that obtained from the proximity effect and other observational constraints. Details of how we identify galaxy formation and follow the motions of formed galaxies have been described in Cen & Ostriker (1993a). Note that in this simulation supernova energy feedback from aging massive stars into the intergalactic medium is not included.

3. Correlation Measures

We analyze the clustering properties of Ly α clouds along the line of sight at $z = 3$ using six different two-point correlation functions: $\xi_{\rho_d}(r)$, $\xi_{\rho_b}(r)$, $\xi_{flux}(v)$, $\xi_{\tau,c}(v)$, $\xi_{\tau,s}(v)$, and $\xi_{line}(v)$. They are defined as follows.

$$\xi_{\rho_x}(r) \equiv \frac{\langle \rho_x(r+r')\rho_x(r') \rangle}{\langle \rho_x \rangle^2} - 1 \quad , \quad (1)$$

where $\xi_{\rho_x}(r)$ is the two-point correlation function (Peebles 1980) of the cold dark matter density ($x = d$) or baryonic density ($x = b$); $\rho_x(r)$ is the density at point r along the line of sight; $\langle \rho_x \rangle$ is its mean averaged over all lines of sight sampled. The angular brackets in the numerator indicate averaging over all pairs of pixels with the line of sight separation between r and $r + \Delta r$. Note that for $\xi_{\rho_d}(r)$ and $\xi_{\rho_b}(r)$ we ignore the peculiar velocity along

the line of sight so that the resulting correlations reflect the more fundamental matter correlations in real space. This fundamental correlational measure will be compared with other measures, which are directly observable and calculated in velocity space, including the peculiar velocity as well as the thermal effect.

The two-point correlation function of the normalized transmitted flux $F(v)$ along the line of sight, $\xi_{flux}(v)$, is defined by

$$\xi_{flux}(v) \equiv \frac{\langle F(v+v')F(v') \rangle}{\langle F \rangle^2} - 1 \quad , \quad (2)$$

where $\langle F \rangle$ is its mean averaged over all lines of sight sampled and the angular brackets in the numerator indicate averaging over all pairs of pixels with the line of sight separation between v and $v + \Delta v$. Note that this flux correlation measure has a slightly different definition than another flux correlation measure used in MCOR (see equation 2 of MCOR for definition).

Next, we propose a new two-point correlation function of (modified) optical depth along the line of sight, defined as

$$\xi_{\tau,c}(v) \equiv \frac{\langle \tau_c(v+v')\tau_c(v') \rangle}{\langle \tau_c \rangle^2} - 1 \quad , \quad (3)$$

$\langle \tau_c \rangle$ is its mean τ_c averaged over all lines of sight sampled the angular brackets in the numerator indicate averaging over all pairs of pixels with the line of sight separation between v and $v + \Delta v$. $\tau_c(v)$ is *not* the optical depth as observed, but is the latter modified as:

$$\tau_c(v) \equiv \text{Min}[\tau_{max}, \tau_{obs}(v)] \quad , \quad (4)$$

where $\tau_{obs}(v)$ is what is directly measured observationally, related to the normalized transmitted flux by $\tau(v) = -\log[F(v)]$; $\text{Min}()$ is the minimum operator, which takes the

smaller of its two arguments. The letter "c" in the subscript of τ_c and $\xi_{\tau,c}$ is intended to stand for "ceiling", imposed on τ_{obs} (equation 4). Because of this notation, we may call $\xi_{\tau,c}$ "capped optical depth correlation function". We use three values of $\tau_{max} = (2.0, 4.0, \infty)$. Note that in the case $\tau_{max} = \infty$, $\tau_c(v) = \tau_{obs}(v)$. The purpose of choosing several τ_{max} 's is to study the dependence of clustering strength on regions with different optical depth, different column densities.

We propose another new two-point correlation function of (yet another modified) optical depth along the line of sight, defined as

$$\xi_{\tau,s}(v) \equiv \frac{\langle \tau_f(v+v')\tau_f(v') \rangle}{\langle \tau_f \rangle^2} - 1 \quad , \quad (5)$$

where $\tau_f(v)$ is defined as:

$$\tau_f(v) \equiv \begin{cases} 1, & \text{if } \tau_{obs}(v) \geq \tau_{min} \\ 0, & \text{if } \tau_{obs}(v) < \tau_{min} \end{cases} \quad (6)$$

We pick three values of $\tau_{min} = (1.0, 2.0, 4.0)$, for a similar intention to study the dependence of clustering strength on the different regions but in a somewhat different angle than $\xi_{\tau,c}$. The letter "s" in the subscript of τ_f and $\xi_{\tau,s}$ is intended to stand for "step", imposed on τ_{obs} (equation 6). We will call $\xi_{\tau,s}$ "stepped optical depth correlation function".

Finally, we test the usual line-line two-point correlation function along the line of sight, defined as

$$\xi_{line}(v) \equiv \frac{\# \text{ of pairs with } v \rightarrow v + \Delta v}{\# \text{ of pairs for a random sample with } v \rightarrow v + \Delta v} - 1 \quad , \quad (7)$$

We use the method described in MCOR to identify lines. This method is different from what is used in extracting lines from observed spectra, so a direct comparison between the simulation and observation is not possible at this time.

In all cases the global average $\langle \rangle$ is understood to be the average over our computed sample at a given redshift $\langle \rangle_z$. The purpose of examining several measures of correlation in the Ly α absorption spectra is threefold. First, we wish to understand the relationship between correlations that are directly measured from observed absorption spectra and the fundamental correlation of the underlying matter distribution. For this purpose, we have included $\xi_{\rho_d}(r)$ and $\xi_{\rho_b}(r)$. Second, we attempt to find a correlational measure which is relatively free from post-observation fitting procedures such as line profile fitting and line deblending, and is relatively insensitive to small changes in observational accuracy in terms of signal to noise ratio and FWHM. For this reason, we have calculated $\xi_{flux}(v)$, $\xi_{\tau,c}(v)$ and $\xi_{\tau,s}(v)$. Each of these three measures is directly based on the observed flux distributions and does not require any fitting procedure. Furthermore, we expect that, once the resolution of observations becomes higher than the width caused by the expected thermal broadening, these measures will be rather robust. This property is in sharp contrast with that of line correlations, for which ambiguity exists in deblending lines regardless of how high a signal to noise ratio an observation can achieve. Third, we want to understand the implications of available observational results obtained by employing the line-line two-point correlation function. Therefore, we also examine the simulation using line-line two-point correlation function $\xi_{line}(v)$, although a direct comparison with observations is still not possible due to differences between the line identification algorithms used in observations and in simulations.

For the first two correlations, ξ_{ρ_d} and ξ_{ρ_b} , no observational noise is added and their validity in a specific cosmological model only depends on the accuracy of the simulation, which is primarily limited by the simulation resolution and box size (and of course additionally by the residual uncertainty in the underlying cosmological model). For the remaining four correlational measures we generate two sets of spectra with (S/N=10, FWHM=30km/s) and (S/N=50, FWHM=6km/s). A sampling bin of 2km s^{-1} is used in all

cases. Since we are interested in regions with large amount of absorption (“clouds”) as well as those with mild amount of absorption (weak lines or “voids”), the widely used Gaussian statistic of noise is not valid, in general. We use the Poisson statistic of noise, which is valid in both low and high flux regions assuming that we know the signal to noise level at each pixel of a spectrum and is identical to the Gaussian statistic in the limit of large photon numbers. This is done in the following manner.

First, we require that the average flux decrement in the simulated spectra, $\langle D \rangle = 1 - \langle \exp^{-\tau_{Ly\alpha}} \rangle$, be equal to the observed value, $\langle D \rangle_{obs} = 0.36$ at $z = 3$ (Press, Rybicki, & Schneider 1993). This is achieved by adjusting the parameter, $\mu \equiv \frac{(\Omega_{0,b}/0.015h^{-2})}{(h j_H/10^{-12}\text{sec}^{-1})^{1/2}}$ (MCOR), where h is Hubble constant in units of 100km/s/Mpc, $\Omega_{0,b}$ is the mean baryonic density and j_H is the hydrogen photoionization rate. This normalization procedure for the flux distribution is *necessary* in order to fix its overall amplitude, due to the large uncertainties of the observed values of $\Omega_{0,b}$ and j_H . The fitted value of μ is 1.90 for the Λ CDM model. Second, we add noise to the normalized spectrum. By definition, the signal to noise ratio at the continuum is

$$S/N = \frac{N_{src}}{\sqrt{N_{src} + N_{noise}}}. \quad (8)$$

where N_{src} and N_{noise} are the number of source photons at the continuum and the number of noise photons, respectively, per frequency bin. Thus, given S/N and N_{noise} , we can solve equation (8) to get N_{src} . To simplify the illustration (without loss of generality) we assume that N_{noise} is dominated by the detector read noise. This is a good approximation only for bright quasars where the number of sky photons is small (due to a shorter exposure time) compared to the read noise of, say, a CCD detector. For example, the gain of the HIRES CCD detector on the Keck telescope is 6.1 electrons, so the number of photons due to the CCD read noise integrated over 5 spatial pixels (for each frequency bin) is

$N_{CCD} = 5 \times 6.1^2 = 186$. For a $V = 16.5$ mag quasar at 5000Å with 1-hr integration time, there are about 4 photons from the sky per spatial pixel, giving a total count of sky photons per frequency pixel (integrated over the 5 spatial pixels) of only 20 photons (see, e.g., Hu et al. 1995). A frequency bin in the synthetic noise-free spectrum with flux f contains fN_{src} photons. When noise is added, the “observed” number of photons (subtracted by the known CCD read noise) in the frequency bin is

$$N_{obs} = Poisson(fN_{src} + N_{CCD}) - N_{CCD}, \quad (9)$$

where $Poisson(X)$ means a Poisson distributed random number with the mean equal to X . The N_{CCD} value of the HIRES CCD detector is adopted in the calculations.

4. Results

For each correlation function computed we use 12,000 lines of sight each having a length of 1280km/s. Figure 1 shows $\xi_{\rho_b}(r)$ (solid curve) and $\xi_{\rho_d}(r)$ (dashed curve). Note that the two correlations are computed in real space as a function of proper distance, as shown in the bottom horizontal axis. For reference the velocity distance, converted from the proper distance using the relation $v = r H(z)$, where $H(z) = 512\text{km/s/Mpc}$ is the Hubble constant at $z = 3$ for the adopted model, is shown in the top horizontal axis. Note that $1 + \xi$ rather than ξ is shown in the plot in order to display negative values of ξ on a logarithmic scale. We see that both dark matter and gas are highly clustered at scales $\leq 0.1h^{-1}\text{Mpc}$ comoving, with dark matter being more strongly clustered than gas on all scales. This apparently surprising result that baryonic gas density is *anti* biased with respect to dark matter density has been found in all simulations to date beginning with our earliest numerical work (Cen 1992). While no completely satisfactory explanation has been given for this fact

it presumably reflects the greater instability of the dark matter to waves perpendicular to the compression vector. The correlation lengths of the dark matter and gas, defined as the length at which ξ is unity, are $0.63h^{-1}\text{Mpc}$ and $0.46h^{-1}\text{Mpc}$ comoving, respectively. The difference in the clustering between dark matter and gas is enhanced due to the thermal photoheating effect in the baryons. It is noted that the resolution of the simulation is $0.087h^{-1}\text{Mpc}$ (2.5 cells), so numerical smoothing in the gas can not be responsible for the difference seen on scales $\geq 0.1h^{-1}\text{Mpc}$. A significant part of the difference may be due to the small fraction of baryons ($\sim 6\%$ by $z = 3$) which were in the highest peaks and have condensed out of the IGM to form stars irreversibly in the simulation.

Figure 2 shows the flux correlation function $\xi_{flux}(v)$ [defined by equation (2)] for S/N=50, FWHM=6km/s (solid curve) and S/N=10, FWHM=30km/s (dashed curve). We see that the flux correlation depends on the observational resolution at small separations, but does not depend on the observational resolution at large separations. For example, for the two cases with the adopted observational parameters, the correlation strengths at $v = (10, 100)\text{km/s}$ are $\xi_{flux} = (0.20, 0.045)$ and $(0.16, 0.042)$, respectively.

Figure 3 shows the “capped optical depth correlation function” $\xi_{\tau,c}(v)$ [defined by equation (3)] for two sets of observational parameters, S/N=50, FWHM=6km/s (thick curves) and S/N=10, FWHM=30km/s (thin curves). For each case three functions for three optical depth ceiling values are shown: $\tau_{max} = \infty$ (solid curve), $\tau_{max} = 4.0$ (dotted curve) and $\tau_{max} = 2.0$ (dashed curve). Three features are to be noted. First, similar to the flux correlation function (ξ_{flux} , shown in Figure 2), this optical depth correlation function only weakly depends on S/N and FWHM on scales $\geq 40\text{km/s}$. Second, on scales $\leq 40\text{km/s}$ its values start to depend more strongly on S/N and FWHM, presumably due to the dominance of small, dense regions at small scales, which become under-resolved with lower observational resolution and/or sensitivity. Third, the correlation depends strongly

on the imposed ceiling value; a lower ceiling value results in a weaker correlation. In other words, high optical depth, high density regions are more strongly clustered than low optical depth, low density regions on all scales probed here, $1 - 320\text{km/s}$, with the trend that the difference is progressively larger on smaller scales. Note that one side of our simulation box spans a velocity range of 1280km/s , so the reader is reminded that the correlation computed here is only valid for scales $\leq 320\text{km/s}$ (a quarter of the box size), because of the periodic boundary condition. It is noted that the two-point correlation function measured by any of the proposed functions here is underestimated due to the missing density waves larger than our simulation box ($\lambda > 10h^{-1}\text{Mpc}$). Since $\xi(r) \propto P_k k^2 \sin(kr) d \ln k$ and $P_k \sim k^{-2}$ at $\lambda = 10h^{-1}\text{Mpc}$ (and the fiducial power index becomes progressively larger than -2.0 on larger scales) for the adopted model, we expect that the underestimate is of a logarithmic factor, perhaps a factor less than two for the computed correlations on scales $v \leq 300 \text{ km/s}$.

To see separately the effects of thermal broadening and peculiar velocity we show, in Figure 4, the corresponding correlations with only the thermal broadening effect (dotted curves), with only the peculiar velocity effect (dashed curves) and with both effects (solid curves; the same as the thick curves in Figure 3) for the case with $S/N=50$, $\text{FWHM}=6\text{km/s}$. For each case three functions for three optical depth ceiling values are shown: $\tau_{max} = \infty$ (thick curve), $\tau_{max} = 4.0$ (medium curve) and $\tau_{max} = 2.0$ (thin curve). We see that the peculiar velocity of the gas serves to boost correlations on both large ($v \geq 100\text{km/s}$) and small scales ($v < 10\text{km/s}$), but to suppress correlations on intermediate scales. The boost of correlation on small scales by the peculiar velocity produces velocity caustics and the boost on large scales due to peculiar velocity is essentially the "Kaiser Effect" (Kaiser 1987). Since the total number of pairs has to be conserved, the correlation strength on intermediate scales is reduced. The thermal motion alone tends to reduce correlations on all scales. However, coupling of peculiar velocity and thermal motion is not simple. It appears that the correlation is slightly stronger at the intermediate scales $v = 15 - 60\text{km/s}$

when both effects are included than that with either of the effects alone. This result reflects the complicated interplay between thermal motion and peculiar velocity of the gas on the correlation. The result that the correlation function at small scales is reduced when both the thermal and velocity effects are included indicates that velocity caustics are largely removed by the thermal broadening effect. But overall, the two effects do not seem to significantly alter the true correlation of the clouds on scales $\geq 20\text{km/s}$.

Figure 5 shows the “stepped optical depth correlation function” $\xi_{\tau,s}(v)$ [defined by equation (6)] for $S/N=50$, $\text{FWHM}=6\text{km/s}$ (thick curves) and $S/N=10$, $\text{FWHM}=30\text{km/s}$ (thin curves). For each case three functions for three optical depth floor values are shown: $\tau_{min} = 1.0$ (solid curve), $\tau_{min} = 2.0$ (dotted curve) and $\tau_{min} = 4.0$ (dashed curve). We remind the reader that a higher value of τ_{min} means a selection of only higher optical depth regions. We see that, at $\tau_{min} = 1.0$ (solid curves), observational parameters S/N and FWHM do not affect the results on the scale $\geq 30\text{km/s}$, simply because the dominant contributions from regions of optical depths just above the floor value are resolution insensitive. Equivalently stated, these regions are already well resolved even by the quoted lower resolution observations. The situation is somewhat different for higher τ_{min} ’s, where higher S/N and lower FWHM give slightly weaker correlations. This is because lower S/N and higher FWHM observations only pick out relatively higher density, high optical depth regions, which are intrinsically more strongly clustered. On small scales, the observational resolution dependence is seen for all three τ_{min} ’s, where higher S/N and lower FWHM give stronger correlations as expected, which is, of course, directly related to the greater resolving power of the relevant dense regions in high resolution observations. Consistent with results shown in Figure 3, we find here that high optical depth, high density regions are more strongly clustered than lower optical depth, low density regions on all scales probed here, $1 - 320\text{km/s}$.

Similar to Figure 4, Figure 6 shows separately the correlations $\xi_{\tau,s}$ with only thermal broadening (dotted curves), with only the peculiar velocity effect (dashed curves) and with both effects (solid curves; the same as the thick curves in Figure 5). For each case three functions for three optical depth ceiling values are shown: $\tau_{min} = 4.0$ (thick curve), $\tau_{min} = 2.0$ (medium curve) and $\tau_{min} = 1.0$ (thin curve). The reader is reminded that the main difference between $\xi_{\tau,c}$ shown in Figures (3,4) and $\xi_{\tau,s}$ shown in Figures (5,6) is that $\xi_{\tau,c}$ measures the correlation by excluding high density, high optical depth regions, while $\xi_{\tau,s}$ measures the correlation by excluding low density, low optical depth regions. We see that the correlation with peculiar velocity alone has the highest amplitude, the one with thermal motion alone has the lowest amplitude, while the correlation with both effects is intermediate at all scales except $v > 100\text{km/s}$. This result is consistent with the fact that high density regions are more strongly clustered and peculiar velocities tend to enhance the correlation strength by, on average, decreasing the pairwise distance in velocity space (Kaiser 1987).

Finally, we show in Figure 7 the line-line correlation function $\xi_{line}(v)$ [defined by equation (7)] for $S/N=50$, $\text{FWHM}=6\text{km/s}$ (thick curves) and $S/N=10$, $\text{FWHM}=30\text{km/s}$ (thin curves), with a flux threshold $F_t = 0.6$ (see MCOR). For each case three functions for two equivalent widths are shown: $W_t = 10\text{km/s}$ (solid curve), and $W_t = 40\text{km/s}$ (dashed curve). We stress that the correlations on scales $\leq 100 - 200\text{km/s}$ are probably sensitive to the details of the line identification scheme. In particular, we believe that the sharp downturns of the line correlation functions on scales $\leq 100 - 200\text{km/s}$ are, in large part, likely due to the blending of lines adjacent in velocity space. However, the correlations on scales $\geq 200\text{km/s}$ are perhaps more robust and less sensitive to specifics of a line identification method. We therefore focus on scales $200 - 320\text{km/s}$, where the upper limit, corresponding to a quarter of the box size, arises from the fact that our simulation box assumes periodic boundary conditions. We see that a higher W_t results in a stronger

correlation on scales $\geq 200\text{km/s}$. This trend is consistent with observations that there is a gradual progression in clustering strength from weak to strong with increasing column density (Crotts 1989; Cristiani et al. 1997). The results are shown to be insensitive to S/N and FWHM. To examine the dependence of the line-line correlation function on the flux threshold F_t , Figure 8 shows $\xi_{line}(v)$ at $F_t = 0.4$ (solid curve), 0.6 (dotted curve) and 0.8 (dashed curve), each with S/N=50, FWHM=6km/s and $W_t = 10\text{km/s}$. We see that demanding a lower F_t is qualitatively equivalent to demanding a larger equivalent width W_t , as shown in Figure 7.

The above separately displayed results are best presented as summarized in Table 1, where we show the clustering strength of all the correlation measures at separations of 50, 100, 200 and 300km/s (at $z = 3$). All measures use S/N=50, FWHM=6km/s. For ξ_{line} , $W_t = 10\text{km/s}$ is used but we note that results with $W_t = 40\text{km/s}$ are very similar. In addition, two measures for galaxy clustering are shown: “ ξ_{galaxy} ” indicates the galaxy-galaxy correlation strength at $z = 3$ if we assume that the galaxies are (linearly) biased over dark matter by an amount equal to that at $z = 0$, i.e., $b \equiv \sigma_8^{-1} = 1.27$, where σ_8 is the density fluctuation in a top-hat sphere of radius $8h^{-1}\text{Mpc}$ at $z = 0$; ξ_{stable} is obtained by extrapolating the observed $z = 0$ galaxy-galaxy two-point correlation function [$\xi(0) = (r/5.5h^{-1}\text{Mpc})^{-1.8}$] to $z = 3$ assuming stable clustering (i.e. correlation function is fixed in real space). A few points become clear from the table.

First, the cosmological model adopted is interesting in that “ ξ_{galaxy} ” is in agreement with ξ_{stable} at $z = 3$. However, if galaxies at $z = 3$ turn out to be much more strongly clustered than that indicated by ξ_{galaxy} , then a higher bias of galaxies over matter is required (if one adopts this particular cosmological model) and it implies that the stable clustering assumption is invalid, vice versa. Note that this model also reproduces all the observations at $z = 0$ quantitatively well. Second, the flux correlation ξ_{flux} does not represent the true

matter correlation well, partly because of its definition and partly because of the fact that it does not particularly reflect the correlation of dense regions (i.e. “clouds”). Third, the optical depth correlation directly using the observed optical depth [$\xi_{\tau,c}(\infty)$] traces the true correlation of the underlying matter ξ_{ρ_d} well with some moderate anti-bias at scales $\leq 100\text{km/s}$. Removing high optical depth regions significantly reduces the correlation on all scales; $\xi_{\tau,c}(2)$ is about a factor of two smaller than $\xi_{\tau,c}(\infty)$ at all scales. Fourth, the best representation of the matter correlation is achieved by $\xi_{\tau,s}(2)$, which faithfully traces ξ_{ρ_d} on all the scales shown. Since optical depth $\tau = 2$ should be easily identifiable with the current observational sensitivity without much distortion caused by noise, $\xi_{\tau,s}(2)$ may represent the best correlational measure both to compare observations with simulations and to compare correlations of Ly α clouds with correlations of galaxies. We note that a Ly α cloud with a column density of $N = 1 \times 10^{14}\text{cm}^{-2}$ and a Doppler width $b = 25\text{km s}^{-1}$ has a central Ly α optical depth of ~ 3.0 . Therefore, $\xi_{\tau,s}(2)$ measures the spatial correlation of Ly α clouds with column densities $\geq 10^{13-14}/\text{cm}^2$. A τ_{min} less than 2.0 enables us to compute correlations of lower column density clouds. The essential difference between the optical depth based correlation measures and flux based measures is that optical depth directly probes the densities of the clouds, thus a direct measure of density. Finally, we emphasize that the line-line correlation is highly dependent on the details of the line identification scheme. While a comparison between observations and simulations can always be made as long as both are analyzed in the same way using a chosen measure, the difference between the line-line correlational measure, which is almost the sole, used clustering indicator of observed Lyman forest correlations, and $\xi_{\tau,s}(2)$, which represents an alternative to the line-line correlation measure, seems clear. The number of lines identified for a given “true” cloud (which is easy to see in simulations) or a given domain of observed spectra depends on observational resolution and noise as well as post-observation fitting procedures. Even in the limit of infinite observational sensitivity the number of lines determined is not unique,

due to the ambiguity in the line fitting and deblending process. We note that $\xi_{\tau,s}$ picks out high optical depth regions, gives each (uniform) spectral pixel in the selected region equal weight, and measures the correlation of these pixels. In essence, $\xi_{\tau,s}$ is a line-line correlation, if one visualizes each selected spectral pixel as a “line”, but it lacks any ambiguity.

While a direct comparison with available observations is not attempted due to the lack of a common measure, we see a broad consistency. Sargent et al. (1980) find that there is very weak correlation on scales $300 - 30,000\text{km/s}$ with an observational $\text{FWHM} \sim 50\text{km/s}$ at $z = 1.7 - 3.3$. Webb (1986) finds a correlation strength of 0.32 ± 0.08 for $\Delta v = 50 - 290\text{km/s}$ with $\text{FWHM} \sim 20\text{km/s}$ at $z = 1.9 - 2.8$. Meiksin & Bouchet (1995) find positive correlations, with a maximum amplitude of $0.5 - 1.0$, on the scales $\Delta v = 100 - 600\text{km/s}$ with $\text{FWHM} \sim 25\text{km/s}$ at $z = 2 - 4$. Rauch et al. (1992) show that there is no strong clustering on all scales probed, $\Delta v > 100\text{km/s}$ with $\text{FWHM} \sim 20\text{km/s}$ at $z = 2.7 - 3.4$. Cristiani et al. (1997) conclude that there is significant clustering at $\Delta v < 300\text{km/s}$ with $\text{FWHM} \sim 10\text{km/s}$ at $z \sim 3.0$, with $\xi \sim 0.6$ at $\Delta v = 100\text{km/s}$ for clouds with $N_{HI} \geq 10^{13.8}\text{cm}^{-2}$, and no significant clustering for $N_{HI} \leq 10^{13.6}\text{cm}^{-2}$.

5. Discussion and Conclusions

Examination of several measures of the correlation of $\text{Ly}\alpha$ clouds and comparison between them and fundamental matter correlations shows that mass is more strongly clustered than that of $\text{Ly}\alpha$ clouds, on all scales at $z = 3$. It is also found that, among the $\text{Ly}\alpha$ clouds, higher density, higher optical depth, higher column density regions are more strongly clustered than lower density, lower optical depth, lower column density regions, with the difference being larger at small separations and smaller at large separations. These effects should be observable even in the current observations. Although we are not able to make a direct comparison with available observations due to the lack of a common

measure, we see a broad consistency between our simulation results and observations. If we assume that galaxies form preferentially in regions whose densities are much higher than those of the Ly α clouds, especially at the redshift considered here, then a consistent picture emerges: the correlation strength for a given set of objects is positively correlated with their characteristic global density and the differences among the correlations of galaxies, Ly α clouds and mass reflect the differences in density that each trace. The property might be traceable to the nature of Gaussian density field where higher density peaks are more strongly clustered than lower density peaks (Bardeen et al. 1986).

The true correlation strength of the matter is about 0.2 – 2.0 on scales 50 – 300km/s, where it can be measured reliably in our simulations, at $z = 3$. Significant positive correlations with a strength of 0.1 – 1.0 are predicted for Ly α clouds in the velocity range 50 – 300km/s. All correlation functions examined here decrease monotonically with increasing separation. Due to our limited box size ($10h^{-1}$ Mpc) the computed correlation underestimates the true correlation. However, the underestimate is expected to be a factor less than two at $v \sim 300$ km/s and smaller at smaller scales. While our limited simulation box size hampers our ability to study the correlations of the Ly α forest on scales $\geq 2.5h^{-1}$ Mpc ($\Delta v = 320$ km/s), we expect that the correlation strength of Ly α clouds on scales ≥ 300 km/s is small, ≤ 0.1 . The correlation strength on scales of several hundred km/sec measures the power of the density fluctuations on comoving megaparsec scales. Thus, an accurate determination of the correlation strength on scales of several hundred km/sec provides a unique data point for the power spectrum on comoving megaparsec scales.

Among the measures examined, the “stepped optical depth correlation function” (Equation 5) seems to be the most useful correlational measure. It reasonably represents the true correlation of the underlying matter, thus enabling a better indication of both matter

correlation and the relationship between galaxies and Ly α clouds. Moreover, it appears to provide a simple alternative to the conventional line-line correlation function with a few obviously advantageous features: 1) it does not require ambiguous post-observation line fitting and deblending procedures such as those commonly employed in the conventional line finding methods, 2) it does not depend sensitively on the observational resolution such as FWHM, once a “true” cloud (which is hard to define observationally but easy to identify and study in three-dimensional simulations) is resolved (this typically means that an FWHM is sufficiently smaller than the thermal broadening width of a cloud) and, 3) it can be easily measured with the current observational sensitivity without being contaminated significantly by the presence of noise, if one chooses an appropriate optical depth floor value τ_{min} , say, ≤ 2.0 .

Applying the newly proposed correlational measures, particularly, $\xi_{\tau,s}(v)$ [defined by equation (5)], to observed spectra, both along the line of sight and in the perpendicular direction for nearby sightlines, will perhaps yield much more unambiguous results about the spatial clustering of the observed Ly α clouds. Comparison of correlations between observed and model spectra employing such a simple unambiguous measure might enable a much simpler interpretation of some essential issues such as if the clouds are made of smaller dense cloudlets.

Aside from the choice of a particular cosmological model which seems viable, the critical ingredient in our simulation is the assumption that the ionizing radiation field is spatially uniform. While it seems reasonable, future larger simulations with box size $\geq 20h^{-1}\text{Mpc}$ are required in order to study correlations up to the scale $5h^{-1}\text{Mpc}$. Such a study will shed light on the origin of the correlations of Ly α forest and possibly also on the properties of the meta-galactic UV background, when compared with observations.

The work is supported in part by grants NAG5-2759, AST91-08103 and ASC93-18185.

REFERENCES

- Bahcall, J.N., et al. 1996, ApJ, 457, 19
- Bardeen, J.M., Bond, J.R., Kaiser, N., & Szalay, A.S. 1986, ApJ, 304, 15.
- Bond, J. R., Szalay, A. S., & Silk, J. 1988, ApJ, 324, 627
- Carswell, R. F., Lanzetta, K. M., Parnell, H. C., & Webb, J. K., 1991, ApJ, 371, 36
- Cen, R. 1992, ApJS, 78, 341
- Cen, R., & Ostriker, J.P. 1993a, ApJ, 417, 404
- Cen, R., & Ostriker, J.P. 1993b, ApJ, 417, 415
- Cen, R., Gnedin, N.Y., & Ostriker, J.P. 1993, ApJ, 417, 387
- Cen, R., Miralda-Escudé, J., Ostriker, J. P., & Rauch, M. 1994, ApJ, 437, L9
- Cristiani, S., D’Odorico, S., Fontana, A., Giallongo, E., & Savaglio, S. 1995, MNRAS, 273, 1016
- Cristiani, S., D’Odorico, S., D’Odorico, V., Fontana, A., Giallongo, E., & Savaglio, S. 1997, MNRAS, 285, 209
- Crotts, A.P.S. 1989, ApJ, 336, 550
- Edelson, & Malkan 1986, ApJ, 308, 59
- Hernquist, L., Katz, N., & Weinberg, D.H. 1996, ApJ, 457, L51
- Hu, E. M., Kim, T.-S., Cowie, L. L., Songaila, A., & Rauch, M. 1995, AJ, 110, 1526
- Kaiser, N. 1987, MNRAS, 227, 1

- Lanzetta, K.M., Bowen, D.V., Tytler, D., & Webb, J.K. 1995, ApJ, 442, 538
- Meiksin, A., & Bouchet, F.R. 1995, ApJ, 448, L85
- Miralda-Escudé, J., Cen, R., Ostriker, J. P., & Rauch, M. 1996, ApJ, 471, 582
- Ostriker, J.P., & Steinhardt, P. 1995, Nature, 377, 600
- Peebles, P.J.E 1980, *The Large-Scale Structure of the Universe* (Princeton: Princeton University Press)
- Petitjean, P., Webb, J. K., Rauch, M., Carswell, R. F., & Lanzetta, K., 1993, MNRAS, 262, 499
- Press, W. H., Rybicki, G. B., & Schneider, D. P. 1993, 414, 64
- Rauch, M., Carswell, R. F, Chaffee, F. H., Foltz, C. B., Webb, J. K., Weymann, R. J., Bechtold, J., & Green, R. F. 1992, ApJ, 390, 387
- Sargent, W.L.W., Young, P.J., Boksenberg, A., & Tytler, D. 1980, ApJS, 42, 41
- Scalo, J.M. 1986, Fund. Cosmic Phys., 11, 1
- Schneider, D.P., et al. 1993, ApJS, 87, 45
- Tytler, D., Fan, X.-M., Burles, S., Cottrell, L., Davis, C., Kirkman, D., & Zuo, L. 1995, in *QSO Absorption Lines*, Proc. ESO Workshop, ed. G. Meylan (Heidelberg: Springer), p. 289
- Walker, T.P., Steigman, G., Schramm, D.N., Olive, K.A., & Kang, H.S. 1991, ApJ, 376, 51
- Webb, J.K. 1986, in IAU Symp. 124, *Observational Cosmology*, ed. A. Hewitt, G. Burbidge, & L.Z. Fang (Dordrecht: Reidel), 803
- Zhang, Y., Anninos, P., & Norman, M.L. 1995, ApJ, 453, L57

Fig. 1.— shows $\xi_{\rho_b}(r)$ (solid curve) and $\xi_{\rho_d}(r)$ (dashed curve). Note that the two correlations are computed in real space as a function of proper distance, as shown in the bottom horizontal axis. For reference velocity distance, converted from the proper distance using the relation $v = r/H(z)$, where $H(z) = 512\text{km/s/Mpc}$ is the Hubble constant at $z = 3$ for the adopted model, is shown in the top horizontal axis. Note that $1 + \xi$ rather than ξ is shown in the plot in order to display negative values of ξ in the logarithmic scale.

Fig. 2.— shows the flux correlation function $\xi_{flux}(v)$ [defined by equation (2)] for two sets of observational parameters, S/N=50, FWHM=6km/s (solid curve) and S/N=10, FWHM=30km/s (dashed curve).

Fig. 3.— shows the “capped optical depth correlation function” $\xi_{\tau,c}(v)$ [defined by equation (3)] for two sets of observational parameters S/N=50, FWHM=6km/s (thick curves) and S/N=10, FWHM=30km/s (thin curves). For each case three functions for three optical depth ceiling values are shown: $\tau_{max} = \infty$ (solid curve), $\tau_{max} = 4.0$ (dotted curve) and $\tau_{max} = 2.0$ (dashed curve).

Fig. 4.— shows the “capped optical depth correlation function” $\xi_{\tau,c}(v)$ [defined by equation (3)] with only thermal broadening (dotted curves), only the peculiar velocity effect (dashed curves) and both effects (solid curves; the same as the thick curves in Figure 3) for the case with S/N=50, FWHM=6km/s. For each case three functions for three optical depth ceiling values are shown: $\tau_{max} = \infty$ (thick curve), $\tau_{max} = 4.0$ (medium curve) and $\tau_{max} = 2.0$ (thin curve).

Fig. 5.— shows the “stepped optical depth correlation function” $\xi_{\tau,s}(v)$ [defined by equation (5)] for two sets of observational parameters S/N=50, FWHM=6km/s (thick curves) and S/N=10, FWHM=30km/s (thin curves). For each case three functions for three optical

depth floor values are shown: $\tau_{min} = 1.0$ (solid curve), $\tau_{min} = 2.0$ (dotted curve) and $\tau_{min} = 4.0$ (dashed curve).

Fig. 6.— shows the “stepped optical depth correlation function” $\xi_{\tau,s}(v)$ [defined by equation (5)] with only thermal broadening (dotted curves), only the peculiar velocity effect (dashed curves) and both effects (solid curves; the same as the thick curves in Figure 5). For each case three functions for three optical depth ceiling values are shown: $\tau_{min} = 4.0$ (thick curve), $\tau_{min} = 2.0$ (medium curve) and $\tau_{min} = 1.0$ (thin curve).

Fig. 7.— shows the line-line correlation function $\xi_{line}(v)$ [defined by equation (7)] for two sets of observational parameters S/N=50, FWHM=6km/s (thick curves) and S/N=10, FWHM=30km/s (thin curves), with a flux threshold $F_t = 0.6$ (see MCOR). For each case three functions for two equivalent widths are shown: $W_t = 10\text{km/s}$ (solid curve), and $W_t = 40\text{km/s}$ (dashed curve).

Fig. 8.— shows $\xi_{line}(v)$ at $F_t = 0.4$ (solid curve), 0.6 (dotted curve) and 0.8 (dashed curve), each with S/N=50, FWHM=6km/s and $W_t = 10\text{km/s}$.

Table 1. Summary of correlations

Δv (km/s)	Δx (h^{-1} Mpc ^a)	ξ_{ρ_d}	ξ_{ρ_b}	ξ_{flux}	$\xi_{\tau,c}(\infty)$	$\xi_{\tau,c}(2)$	$\xi_{\tau,s}(2)$	ξ_{line}	“ ξ_{galaxy} ” ^c	ξ_{stable} ^d
50	0.39	1.6	1.1	0.10	0.95	0.43	1.58	−0.35 ^b	2.0	1.83
100	0.78	0.70	0.40	0.050	0.34	0.17	0.57	0.15 ^b	0.89	0.52
200	1.56	0.20	0.20	0.007	0.16	0.06	0.16	0.36	0.25	0.15
300	2.34	0.20	0.20	0.005	0.06	0.03	0.10	0.11	0.25	0.073

^acomoving length units

^bprobably underestimated due to line blending

^cgalaxy correlation at $z = 3$ derived from ξ_{ρ_d} assuming a linear density bias of $1.27 = 1/\sigma_8$

^dgalaxy correlation at $z = 3$ derived by extrapolating present observed galaxy correlation function to $z = 3$ assuming stable clustering

Figure 1

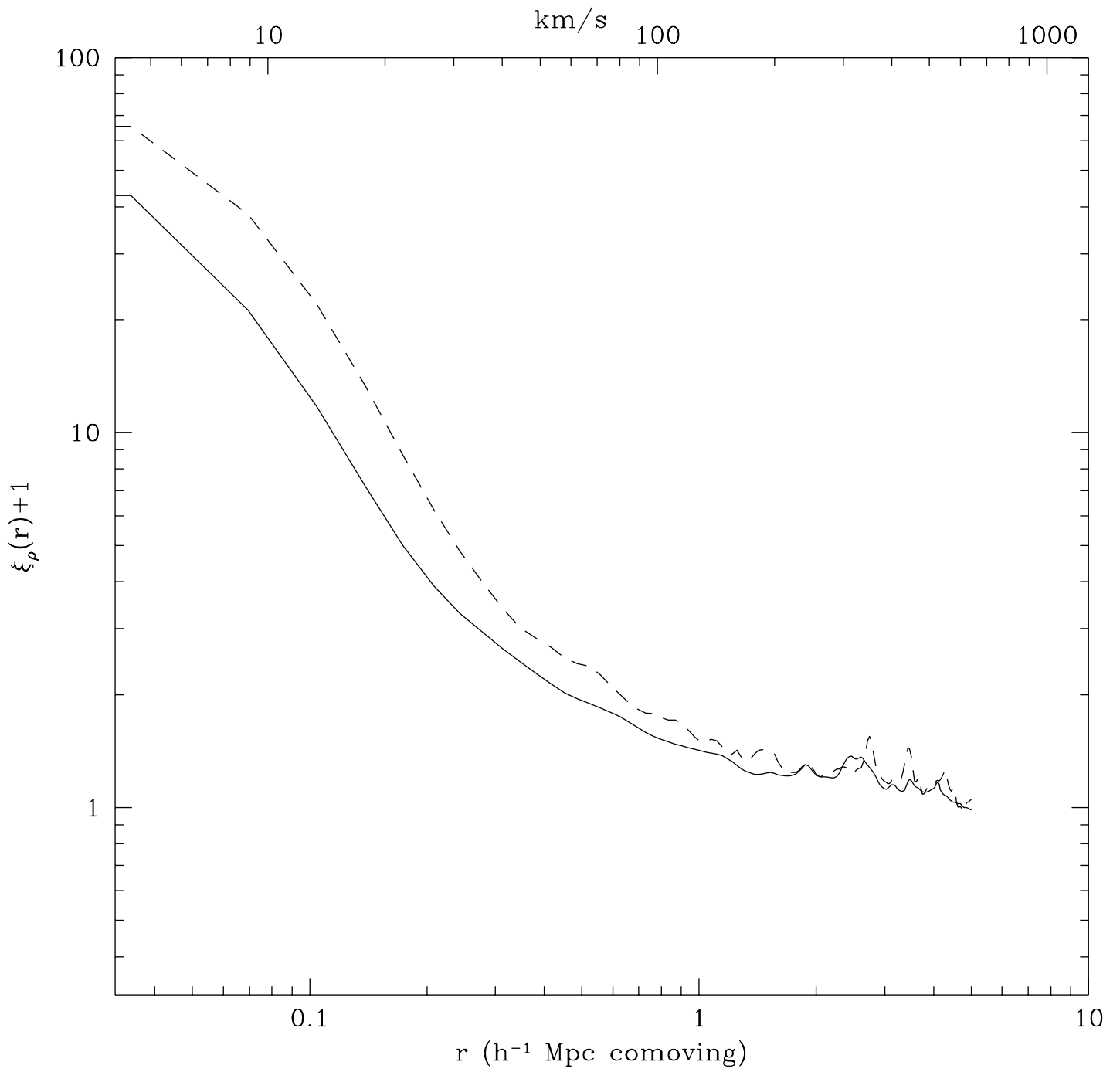


Figure 2

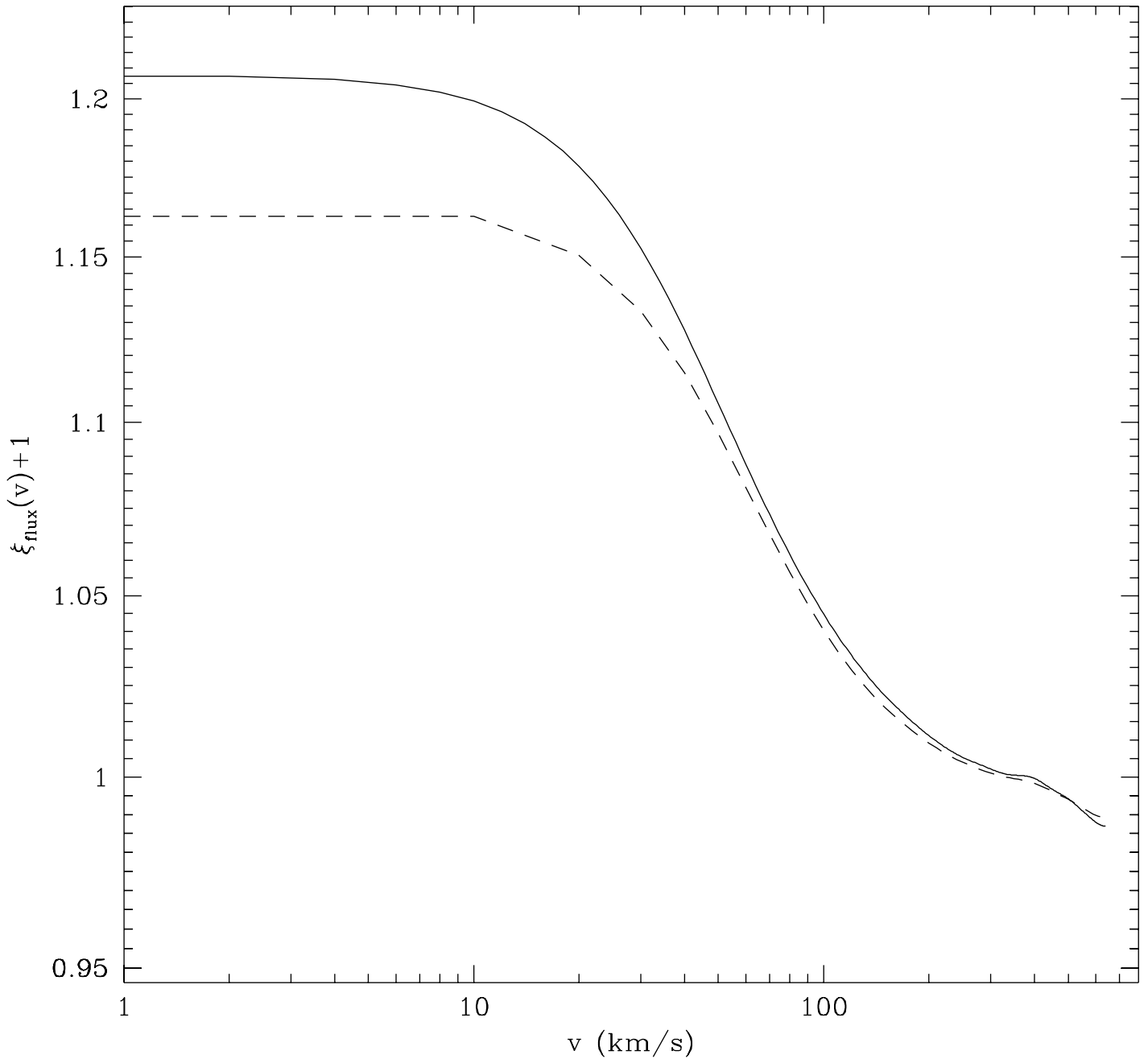


Figure 3

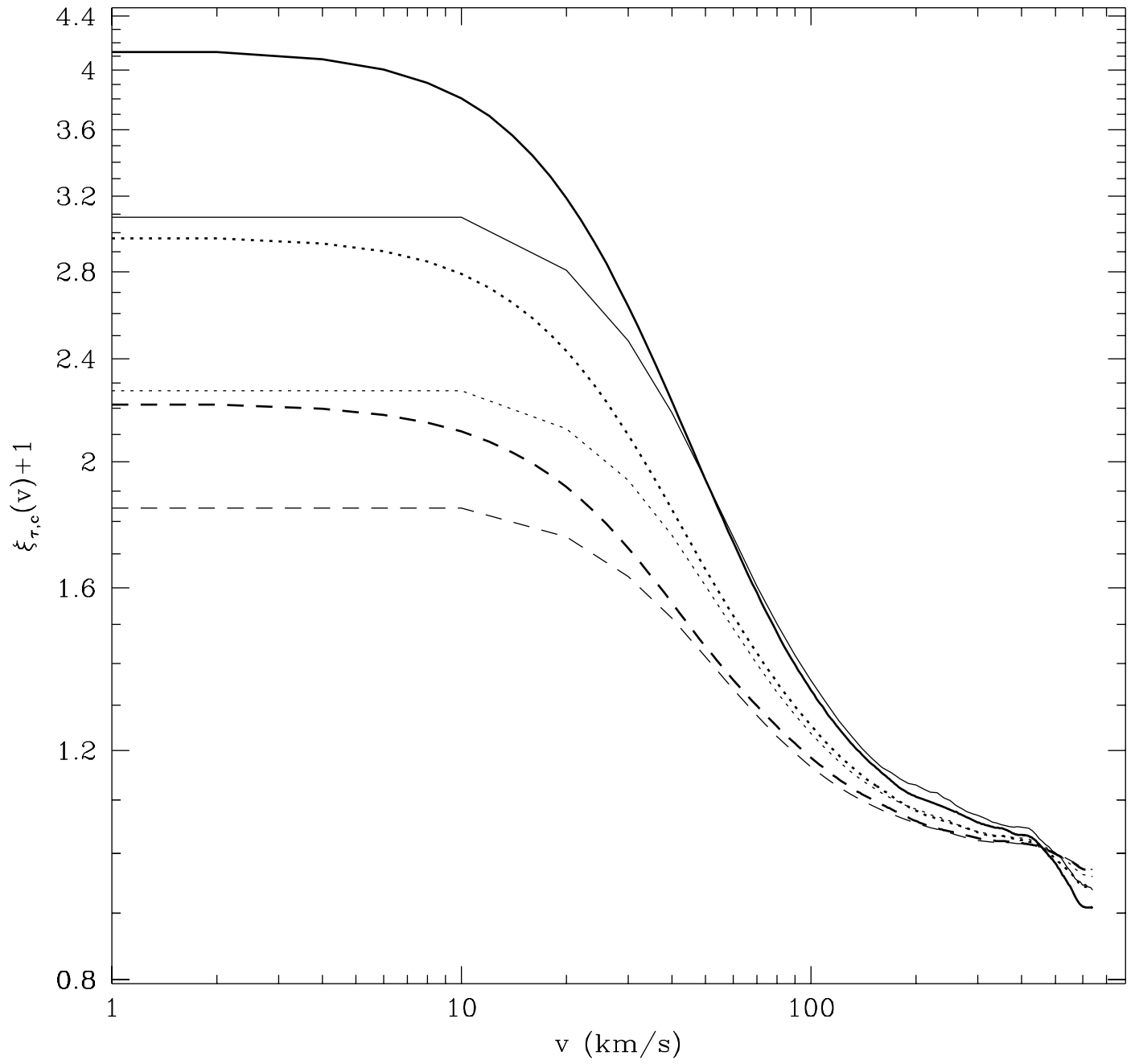


Figure 5

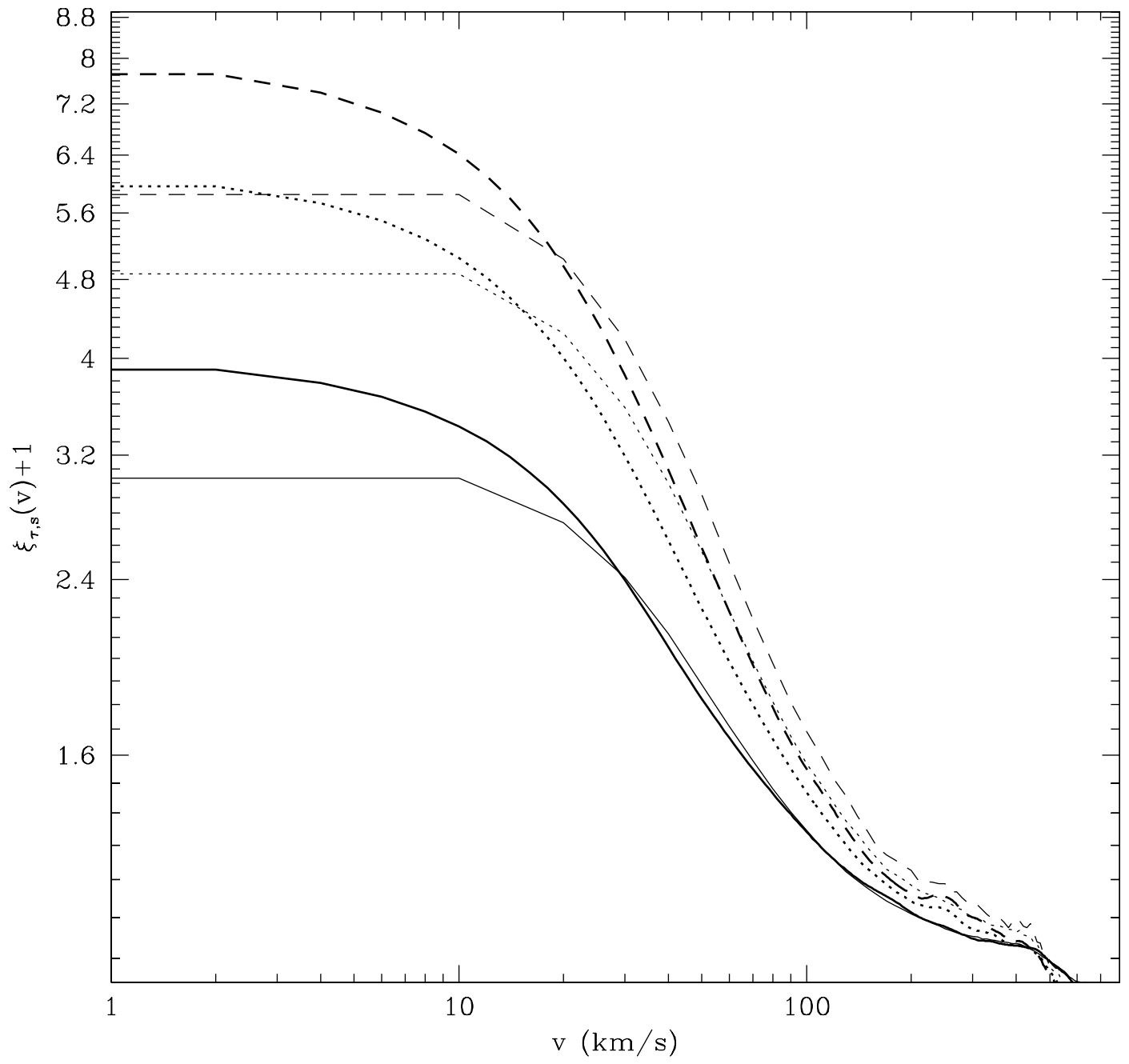


Figure 7

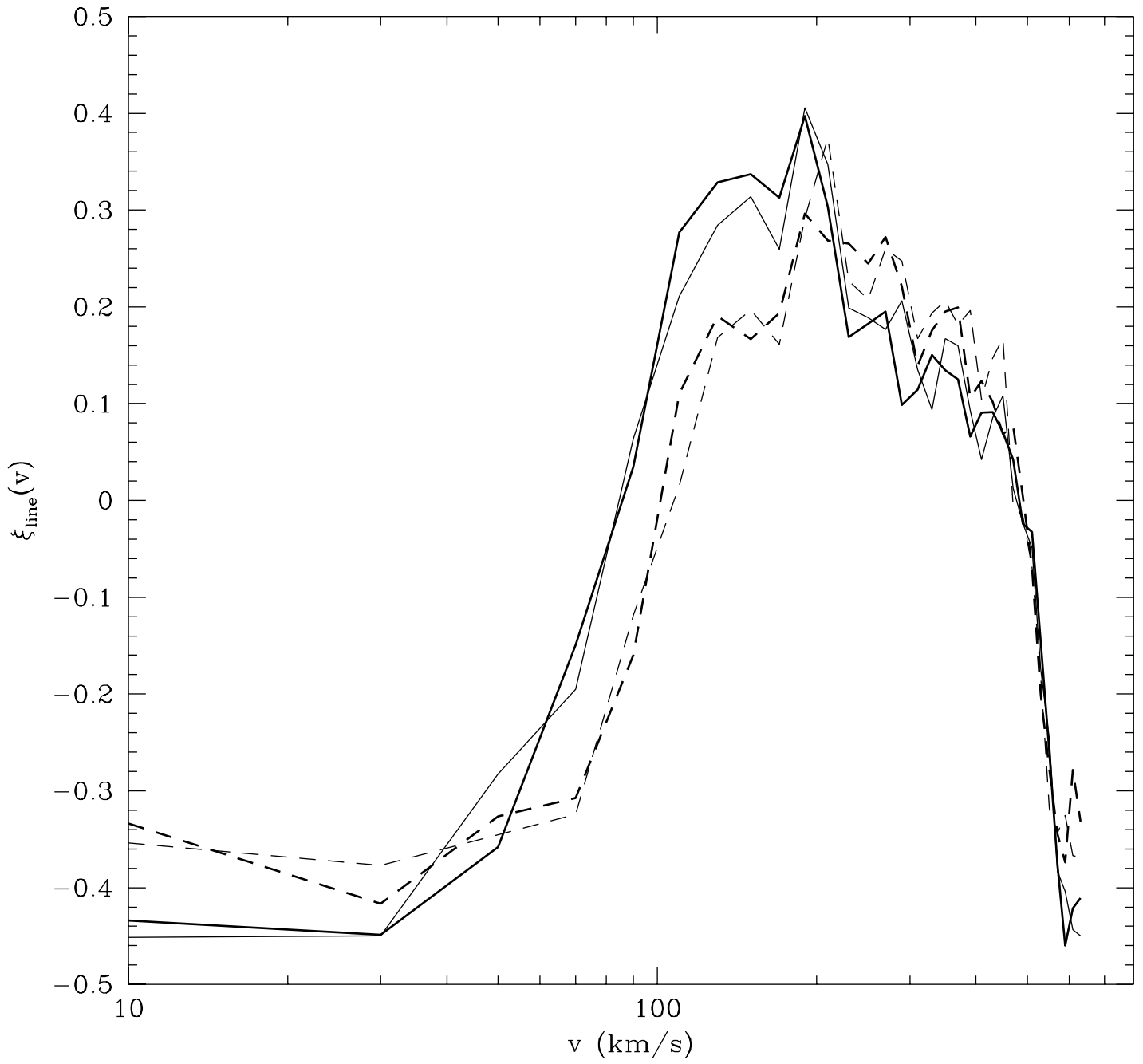


Figure 8

